Selective isolation of mouse glial nuclei optimized for reliable downstream omics analyses

Miguel A. Pena-Ortiz[1†], Sarfraz Shafiq[1†], Megan E. Rowland[2] and Nathalie G. Bérubé[1*]

Affiliations:

[1]Departments of Anatomy and Cell Biology, Paediatrics, and Oncology, Schulich School of Medicine and Dentistry, Western University, London, ON, Division of Genetics and Development, Children's Health Research Institute, London, ON.

[2]Department of Biochemistry and Molecular Biology, The University of British Columbia, Vancouver, BC.

[†] These authors contributed equally to this work.

[*] Corresponding author: Nathalie G. Bérubé (nberube@uwo.ca)

Short title: Isolation of glial nuclei from mouse brain

Abbreviations:

AST, astrocyte; BSC, back scatter; DAPI, 4′,6-diamidino-2-phenylindole; DEPC, diethyl pyrocarbonate; DNA, deoxyribonucleic acid; DTT, dithiothreitol; FACS, fluorescence-activated cell sorting; FANS, fluorescence-activated nuclei sorting; FSC, forward Scatter; GFP, green fluorescent protein; MACS, magnetic-activated cell sorting; MG, microglia; OLs, oligodendrocytes; OPCs, oligodendrocyte precursor cells; PBS, phosphate buffered saline; RIN, RNA integrity number; RNA, ribonucleic acid

Highlights

- Fast and easy isolation and sorting of glial nuclei from the mouse brain

- Reproducible and versatile processing of enriched nuclei for omics applications

ABSTRACT

Background

Isolation of cell types of interest from the brain for molecular applications presents several challenges, including cellular damage during tissue dissociation or enrichment procedures, and low cell number in the tissue in some cases. Techniques have been developed to enrich distinct cell populations using immunopanning or fluorescence activated cell/nuclei sorting. However, these techniques often involve fixation, immunolabeling and DNA staining steps, which could potentially influence downstream omics applications.

New Method

Taking advantage of readily available genetically modified mice with fluorescent-tagged nuclei, we describe a technique for the purification of cell-type specific brain nuclei, optimized to decrease sample preparation time and to limit potential artefacts for downstream omics applications. We demonstrate the applicability of this approach for the purification of glial cell nuclei and show that the resulting cell-type specific nuclei obtained can be used effectively for omics applications, including ATAC-seq and RNA-seq.

Results

We demonstrate excellent enrichment of fluorescently-tagged glial nuclei, yielding high quality RNA and chromatin. We identify several critical steps during nuclei isolation that help limit nuclei rupture and clumping, including quick homogenization, dilution before filtration and loosening of the pellet before resuspension, thus improving yield. Sorting of fluorescent nuclei can be achieved without fixation, antibody labelling, or DAPI staining, reducing potential artifactual results in RNA-seq and ATAC-seq analyses. We show that reproducible glial cell type-specific profiles can be obtained in transcriptomic and chromatin accessibility assays using this rapid protocol.

Comparison with existing methods

Our method allows for rapid enrichment of glial nuclei populations from the mouse brain with minimal processing steps, while still providing high quality RNA and chromatin required for reliable omics analyses.

Conclusions

We provide a reproducible method to obtain nucleic material from glial cells in the mouse brain with a quick and limited sample preparation.

KEYWORDS

Glia

Nuclei isolation

Fluorescence-activated sorting

Mouse brain

Omics

1. INTRODUCTION

Glial cells regulate essential processes of the central nervous system during development and in the adult brain like myelination, immune response, dendritogenesis, neuromodulation, and synapse formation, maturation and elimination (Matejuk and Ransohoff, 2020; Vainchtein and Molofsky, 2020). Of the different glial cells, astrocytes, oligodendrocytes and microglia are the most studied, due to their different roles in the nervous system physiology and disease (Allen and Lyons, 2018). Astrocytes directly form signalling networks with neurons (Durkee and Araque, 2019) and are therefore integral to nervous tissue function, including synapse formation and maintenance (Allen and Eroglu, 2017). Microglia are the resident immune cells of the brain but also participate in neuronal development, synaptogenesis and synapse maturation, through pruning and the release of molecules including nerve growth factor and tumor necrosis factor (Matejuk and Ransohoff, 2020; Reemst et al., 2016). Oligodendrocyte precursor cells (OPCs) not only differentiate into oligodendrocytes responsible for myelination throughout life but are also able to form synapses with neurons and may establish bidirectional communication (Sakry et al., 2014, 2011). Oligodendrocytes form the myelin sheath, regulating conduction across the axon, but can also regulate synaptic transmission through potassium clearance and the release of factors like brain derived neurotrophic factor (Xin and Chan, 2020).

The differentiation, maturation and function of glial cells are tightly regulated by changes in their chromatin and transcriptome (Hammond et al., 2019; Lattke et al., 2021; Marques et al., 2018). Epigenetic changes during development direct cell fate and, after maturation, regulate cellular function through regulation of the transcriptome (Bayraktar et al., 2015; Eggen et al., 2019; Tiane et al., 2019). There is also increasing evidence that continuous and plastic communication exists between different types of glia throughout life, highlighting the need to understand cell type-specific contributions and changes (Domingues et al., 2016; Nutma et al.,

93   2020; Vainchtein and Molofsky, 2020). The exploration of the transcriptome of glial cells and

94   the correlation to chromatin architecture is therefore a key area of investigation that will expand

95   our understanding of the role of these cells in physiological conditions and disease.

96   *In vivo* studies in the mouse brain provide several advantages over culture, the most salient

97   being the ability to amalgamate all signals and their consequences in a complete system.

98   However, *in vivo* molecular studies have been hampered by the heterogeneity of brain tissue,

99   preventing the assignment of particular alterations to specific cell types (Maze et al., 2014).

100   The size of the cell type population is also relevant for glial cells, which tend be fewer

101   compared to neurons, or expression and chromatin differences might be confounded by higher

102   levels in other cell types. Therefore, a necessary step for omics studies of brain cells is to purify,

103   or at least enrich, for a cell type of interest prior to molecular analyses. To this end, several

104   methods have been developed to enrich for particular cell types of interest, include sorting of

105   immunolabelled cells or nuclei of the desired cell type (Douvaras and Fossati, 2015; Holt and

106   Olsen, 2016; John Lin et al., 2017).

107   The first step in many protocols involves an enzymatic digestion to dissociate brain tissue

108   into cell suspensions. The digestion time and type of enzymes must be carefully optimized to

109   minimize loss of antigen targets of antibodies used in subsequent steps (Barres, 2014).

110   Although these methods allow the isolation of whole cells, loss of membrane integrity from

111   sheer stress can induce stress signals and could alter chromatin structure and gene expression

112   profiles (Mo et al., 2015). Once a cell suspension is obtained, different approaches can be used

113   to enrich for a specific cell type. Immunopanning is commonly used for this purpose and

114   involves sequential plating of cell suspensions on antibody-coated plates to deplete cell

115   populations based on membrane markers (Foo et al., 2011). This approach is most suitable to

116   maintain and study these cell populations in culture; however, transcriptional changes are

117   known to occur *in vitro*, and might not reflect the state of the cell prior to cell collection.

118   Alternatively, cells can be either labeled with fluorophore-tagged antibodies and isolated using

119   fluorescence-activated cell sorting (Cahoy et al., 2008; Guez-Barber et al., 2012), or labeled

120   with magnetically tagged antibodies and isolated with magnetic-activated cell sorting (MACS,

121   (Marek et al., 2008). Although these methods allow good enrichment of populations, changes

122   in transcription and chromatin structure could occur due to the initial dissociation steps and

123   prolonged manipulation. Both FACS and MACS require incubation periods with antibodies,

124   and sorting might require long periods of time or multiple elution rounds in the case of MACS

125   (Chongtham et al., 2021). Another limitation is that each glial cell type is itself heterogeneous,

126   making it challenging to find antibodies that will select for all sub-populations. (Marques et

127   al., 2016; Matias et al., 2019). In order to limit disruptions caused by stress response inherent

128   to the cell dissociation step, it is possible to instead quickly dissociate all cell membranes to

129   isolate nuclei (Binek et al., 2019; Chongtham et al., 2021; Mo et al., 2015). Similar to whole

130   cells, cell type -specific nuclei can be labeled with antibodies and sorted. While early studies

131   simply used NeuN to obtain neuronal and non-neuronal populations (Jiang et al., 2008),

132   specific cell-type nuclear markers have been used for oligodendrocytes (Mendizabal et al.,

133   2019) and microglia (Nott et al., 2019). Although changes in the chromatin and transcriptome

134   caused by signals from outside the nuclei would be removed, serial incubations and

135   manipulation may still affect yield by breaking the nuclei.

136   To avoid the use of antibodies, genetic approaches emerged to tag cells or nuclei of interest

137   with fluorescent proteins. The commercially available mice B6;129-Gt(ROSA)26Sor$^{tm5(CAG-}$

138    $^{Sun1/sfGFP)Nat/J}$ (Mo et al., 2015), referred as Sun1-GFP , have a Cre-sensitive green fluorescent

139   protein (GFP) and SUN1 nuclear lamina fusion protein that can be used to fluorescently tag

140   nuclei of interest using cell-type specific Cre lines of mice (Mo et al., 2015). Available

141   protocols for isolation and fluorescence activated nuclei sorting (FANS) require prolonged

142   processing and manipulation before enrichment. To obtain nuclei suspensions, these methods

143   use time-consuming ultracentrifugation, as long as 2.5 h in gradients (Percoll or iodixanol) that

144   might be expensive or not readily available (Jiang et al., 2008). In addition, several protocols

145   stain nuclei with dyes like DAPI or propidium iodide to help remove doublets during sorting

146   that could interfere with downstream applications (Chongtham et al., 2021; Mo et al., 2015).

147   Here, we present a time saving procedure for isolation of fluorescent nuclei that uses a

148   readily available sucrose gradient, and does not require fixation, ultracentrifugation or other

149   prolonged manipulations and incubations. We show that this method is suitable for glial cells,

150   providing high yield of nuclei with limited clumping. Furthermore, high enrichment of

151   fluorescent nuclei using FANS was achieved by removing nuclei doublets without the use of

152   dyes or additional antibodies. Finally, we also show that the enriched nuclei can be used for

153   omics analysis, as RNA sequencing and assay for transposase-accessible chromatin followed

154   by sequencing (ATAC-seq) revealed profiles characteristic of astrocytes,

155   OPCs/oligodendrocytes and microglia. Our simplified workflow limits complications during

156   nuclei enrichment, prevents possible artefacts in downstream applications and provides high

157   quality RNA and chromatin for omics analyses

158

159 **2. MATERIALS AND METHODS**

160 *2.1 Animals*

161 All procedures involving animals were conducted in accordance with the regulations of the

162 Animals for Research Act of the province of Ontario, Canada and approved by the University

163 of Western Ontario Animal Care and Use Committee (2017-048). Mice were exposed to 12-

164 hour light/12-hour dark cycles and fed *ad libitum* with tap water and regular chow.

165 The Sun1-GFP mice were obtained from the Jackson Laboratories (B6;129-

166 Gt(ROSA)26Sor$^{tm5(CAG-Sun1/sfGFP)Nat/J}$, IMSR JAX:021039, MGI:5614796) (Mo et al. 2015).

167 Homozygous Sun1-GFP female mice were mated with male mice heterozygous for the

168 tamoxifen-inducible Cre recombinase gene under the control of promoters specific for each

169 glial cell type used: B6 Glast-CreER (Tg(Slc1a3-cre/ERT)1Nat, IMSR JAX:012586,

170 MGI:4430111) for astrocytes (Slezak et al., 2007), Sox10-CreER (Tg(Sox10-

171 icre/ERT2)388Wdr, IMSR JAX:027651, MGI:5634390) for OPCs (McKenzie et al., 2014),

172 and CX3CR11-CreER (B6.129P2(Cg)-Cx3cr1$^{tm2.1(cre/ERT2)Litt}$/WganJ, ISMR JAX:021160,

173 MGI:5617710) for microglia (Parkhurst et al., 2013).

174 *2.2 Genotyping*

175 Genomic DNA from ear punches was extracted by incubating samples with DirectPCR Lysis

176 Reagent (Viagen 102-T) and Proteinase K at 55°C overnight. DNA was amplified using

177 primers specific to different genetically engineered alleles (Supplementary Table 1) using

178 FroggaMix (FroggaBio FBTAQM). PCR conditions started with 95°C for 3 min, followed by

179 34 cycles of 95°C for 10s, 57°C for 20s and 72°C for 1min, ending with 72°C for 5 minutes.

180 *2.3 Tamoxifen administration*

181 Tamoxifen (10 mg, Sigma T5648) was mixed with 100 µl 95% Ethanol, incubated at 60°C

182 until dissolved and diluted with 900 µl corn oil (Sigma C8267). Tamoxifen was injected

183 intraperitoneally to induce Cre recombinase expression in different glial cell types. For OPCs

184 and oligodendrocytes, Sun1-GFP lactating mothers crossed with Sox10-CreER males were

7

185   injected with 2 mg tamoxifen for three consecutive days; for astrocytes, post-natal day 10

186   Glast-CreER;Sun1-GFP male pups were injected with 1 mg tamoxifen for three consecutive

187   days; for microglia, 6 week-old CX3CR11-CreER;Sun1-GFP male mice were injected with 2

188   mg for five consecutive days.

189   *2.4 Tissue collection and nuclei isolation*

190   Mouse brains were dissected in ice cold phosphate buffered saline (PBS) and samples were

191   frozen on dry ice before being stored at -80°C. Tissue was collected from tamoxifen-treated

192   20-day old Sox10-Cre;Sun1-GFP males (forebrain), 1 month-old Glast-Cre;Sun1-GFP male

193   mice (cortex) and from 2 month-old Cx3cr1-Cre;Sun1-GFP male mice (cortex and

194   hippocampus). For nuclei isolation, the solutions were made fresh before each experiment

195   using DEPC water (diethyl pyrocarbonate, Sigma D5758) and kept on ice. Frozen tissue was

196   homogenized in 500µl of homogenization buffer [*HB*, 20 mM Tricine KOH, 25 mM MgCl2,

197   250 mM sucrose, 1 mM DTT, 0.15 mM spermine, 0.5 mM spermidine, 0.1% IGEPAL-630, 1x

198   protease inhibitor (Millipore Sigma 11873580001), 1 µl/ml RNaseOUT™ RNase inhibitor

199   (Thermo Fisher Scientific 10777019)] with a pestle homogenizer for approximately one minute

200   until a fine suspension was visible. The sample was then diluted to 7.5 ml with HB, filtered

201   through a 40 µm strainer (Falcon 08-771-1) and carefully pipetted over 7.5 ml of cushion buffer

202   [*CB*, 0.5 mM MgCl2, 0.88 M sucrose, 0.5 mM DTT, 1x protease Inhibitor (Millipore Sigma

203   11873580001), 1 µl/ml RNaseOUT™ RNase inhibitor (Thermo Fisher Scientific 10777019)].

204   Samples were centrifuged at 2800 x g for 20 mins at 4°C to pellet nuclei. The supernatant was

205   carefully removed, and the pelleted nuclei were incubated for 10 min in resuspension buffer

206   [*RB*, 500 µl 4% FBS, 0.15 mM spermine, 0.5 mM spermidine, 1 ul/ml RNaseOUT™ RNase

207   inhibitor (Thermo Fisher Scientific 10777019) in PBS] and mixed by gentle pipetting.

208

209

210   *2.5 Fluorescence activated nuclei sorting*

211   Samples were filtered through a 20 μm strainer (pluriStrainer 43-10020-60) before sorting on

212   a Sony SH800 Cell Sorter with a 100 μm nozzle, and the following gains for the sensors:

213   FSC:14, BSC: 35%, FL1(EGFP):38%. Gating is initially set to discard larger events. Next,

214   GFP intensity was plotted against GFP fluorescence area to eliminate doublets and nuclei

215   clusters by discarding events with higher area. From this final gating step, events with lower

216   GFP intensity were discarded to increase purity of the collected nuclei. Sample volumes

217   sometimes needed to be adjusted with RB in order to maintain a constant flow of events per

218   second. Sorting of the sample was paused throughout the session as needed to resuspend the

219   sample and avoid clumping of the nuclei. For RNA extraction, sorting was also paused to mix

220   the sorted nuclei with the lysis buffer in the collection tubes (described below). To assess the

221   enrichment of GFP+ nuclei in the final sorted nuclei population, 5000 to 10000 nuclei were

222   collected in PBS and an aliquot of the suspension was mixed with 1μg/ml DAPI and placed on

223   a glass slide. The proportion of GFP+ nuclei was quantified with an inverted microscope (DMI

224   6000b, Leica) and digital camera (ORCA-ER, Hamamatsu).

225   *2.6 RNA purification and RNA-seq library preparation*

226   Sorted Sun1-GFP$^+$ nuclei were collected in 100 μl lysis buffer from the Single cell RNA

227   purification kit (NorgenBiotek 51800) with 2% β-mercaptoethanol. Immediately after sorting,

228   additional lysis buffer was added to reach 600 μl of total lysate volume, as well as 600 μl 70%

229   ethanol. RNA purification was performed according to the manufacturer's instructions,

230   including an in-column DNase treatment. Samples were eluted twice from the column with 8-

231   12 μl of elution buffer. RNA concentration was determined using Qubit fluorometer

232   (Invitrogen) according to the manufacturer's instructions using 1-2 μl of sample. RNA integrity

233   was determined using an Agilent Bioanalyzer. Libraries from microglia samples were

234   constructed using 35 ng of RNA with the VAHTS Universal V8 RNA-seq Library Prep Kit for

235   Illumina (Vazyme NR605-01), while astrocyte and OPC/oligodendrocyte libraries were made

236   with 90 ng of RNA using VAHTSTM Total RNA-seq (H/M/R) Library Prep Kit for Illumina

237   (Vazyme NR603-01) following the manufacturer's instructions.

238   *2.7 Assay for transposase-accessible chromatin (ATAC)*

239   Approximately 150,000 sorted Sun1-GFP$^+$ nuclei were collected in 50 µl of RNase free PBS.

240   To concentrate the nuclei, the suspension was centrifuged at 3,000 rpm for 5 minutes at 4°C.

241   The supernatant was then carefully removed, and nuclei were resuspended in tagmentation

242   buffer containing Tn5 transposase (Vazyme TD501) for 45 min. at 37°C. Column purification

243   of the samples was quickly performed with QIAquick PCR Purification Kit (Qiagen 28104) to

244   end the tagmentation reaction. Enrichment and purification of the libraries was done according

245   to the TruePrep DNA kit instructions. Quantitative PCR was used to determine the number of

246   enrichment cycles to reach one third saturation, and all the libraries were amplified with more

247   than 12 PCR cycles. Clean-up of all sequencing libraries was performed with SPRIselect beads

248   (Beckman Coulter). The size and purity of the libraries were assessed using an Agilent

249   bioanalyzer before storing at -80°C.

250   *2.8 Deep sequencing and data analysis*

251   Pooled equimolar libraries were sequenced at Canada's Michael Smith Genome Sciences

252   Centre (BC Cancer Research, Vancouver, BC, Canada, https://www.bcgsc.ca) using the

253   Illumina Hiseq (Illumina Inc., San Diego, CA). The libraries were sequenced as a 150 bp paired

254   end run. 50 million paired-end reads were obtained for RNA-seq and 100 million paired-end

255   reads for ATAC-seq. Raw reads were pre-processed using Cutadapt and mapped against Mus

256   musculus GRCm39 with HISAT2 for RNA-seq and bowtie2 for ATAC-seq. SAMtools was

257   used to sort and convert SAM files. Gene abundance for RNA-seq was calculated using

258   StringTie. ATAC-seq peaks were visualized using the Integrative genomic viewer IGV (Broad

259   Institute). Heatmaps of differential gene expression from RNA-seq data were generated using

260   Heatmapper (Babicki et al., 2016) with single linkage hierarchical clustering and spearman

261   rank correlation. Expression enrichment of cell type-specific transcription factors was

262   calculated using the cell type-enriched lists and method described in Zhang et al., 2014. Briefly,

263   by dividing the average for each cell type by the sum of the averages of the other cell types.

264 **3   RESULTS AND DISCUSSION**

265   We used available transgenic mice to obtain brain tissue with GFP tagged nuclei in astrocytes,

266   microglia or OPC/oligodendrocytes. Optimized nuclei isolation was used to obtain nuclei

267   suitable for FANS (Figure 1A). Sorted nuclei were then used for RNA or chromatin extraction,

268   followed by the corresponding procedures for RNA-seq and ATAC-seq (Figure 1B).

269

270
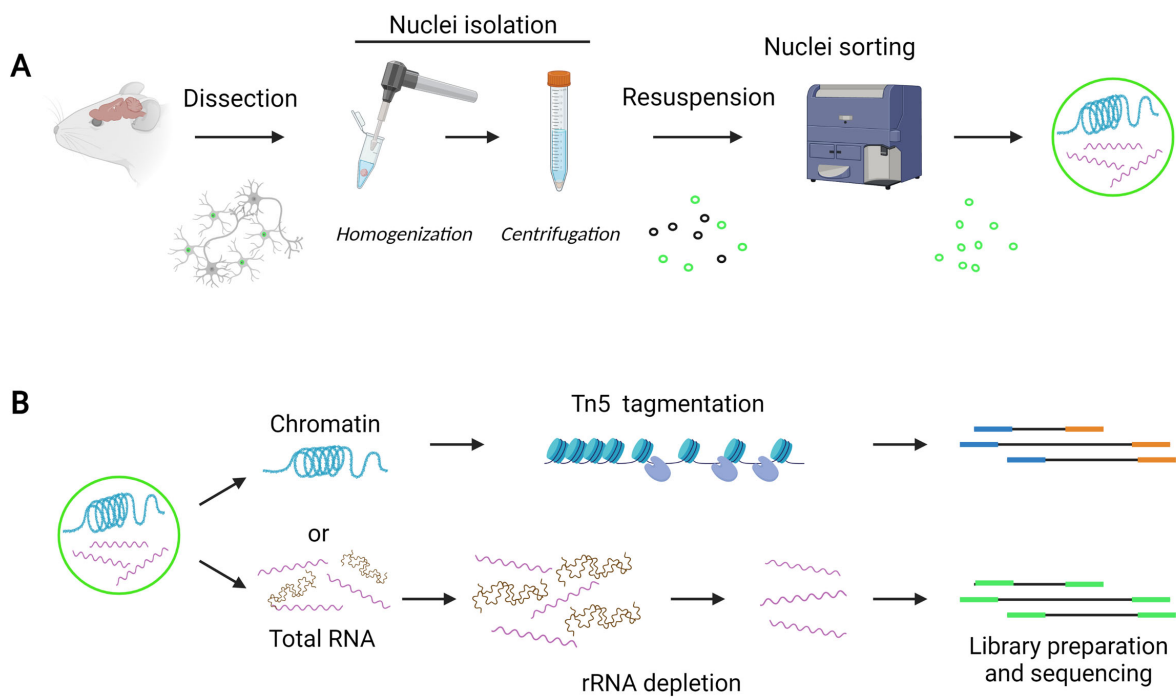
271

272   Figure 1. *Protocol overview*. (A) Tamoxifen-treated mice that express Sun1-GFP in astrocytes,

273   OPC/oligodendrocytes or microglia are sacrificed, and brain tissue dissected and snap frozen.

274   After tissue homogenization, nuclei are isolated by centrifugation and sorted to enrich for

275   Sun1-GFP-tagged nuclei. (B) Sun1-GFP nuclei are immediately processed for total RNA

276   extraction or chromatin accessibility assay (ATAC-seq) using Tn5. Ribosomal RNA is

277   depleted from total RNA samples before generation of the RNA-seq libraries.
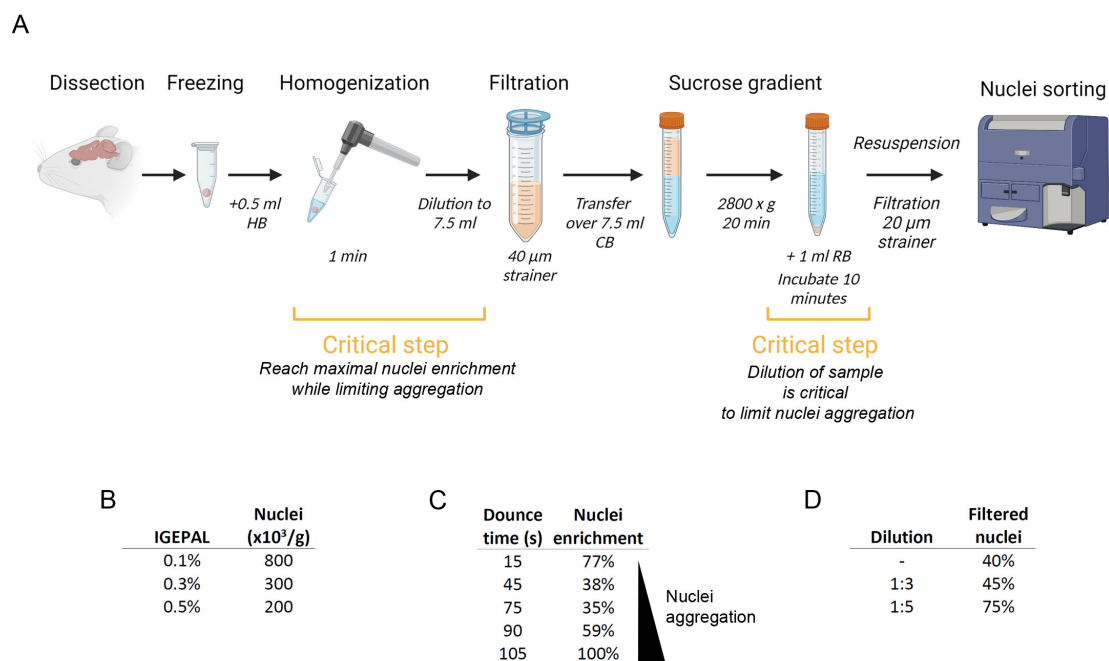
278

279

3.1 Nuclei isolation and sorting

We based this nuclei isolation protocol on the method previously published by (Mo et al., 2015). We observed loss of nuclei through homogenization and centrifugation steps, probably due to astringent conditions that affected nuclei integrity. To address this, we optimized the homogenization step and chose a nuclei pelleting centrifugation with sucrose gradient instead of a iodixanol gradient interlayer collection (Figure 2A). We modified the amount of detergent and length of dounce homogenization to maximize yield and integrity of the nuclei while limiting aggregation and clumping caused by leakage of the intranuclear material from ruptured nuclei (Maitra et al., 2021). To determine optimal detergent concentration and dounce time, frozen cortex tissue was homogenized in HB with 0.1%, 0.3% or 0.5% IGEPAL (Figure 2B). Samples were collected throughout the homogenization, stained with DAPI and quantified under a microscope. We observed that homogenization with 0.1% IGEPAL yielded the maximum number of nuclei with a dounce time of 105 s (Figure 2B and 2C). However, we observed that nuclei aggregation also increased with dounce time, potentially from rupture and leakage of a subset of nuclei. This clumping caused problems in the following steps, as it clogged filters during the filtration steps before sorting and ultimately decreased the final yield. Nuclei aggregates would also affect the sorting step, as they block the line or, if sorted, decrease purity. To prevent clumping of the nuclei, we used a dounce time of 1 min and pipetting was kept to a minimum with all nuclei suspensions. The nuclei yield obtained was enough for downstream applications with no clumping and minimal nuclei loss.

In addition to detergent concentration and dounce time during homogenization, we found that a key step to obtain high yield was dilution of the nuclei suspension prior to filtration. The nuclei dilution at this step prevents clumping, clogging of the strainer and diminishes loss of nuclei. Furthermore, nuclei yield was significantly improved by increasing the dilution of the suspension to 1:5 (Figure 2D). We used an equivalent volume of a sucrose gradient (CB) and

305 pelleted the nuclei, as we found this approach more efficient, cost-effective, and direct than

306 using commercial gradients such as iodixanol. These gradients require ultracentrifugation and

307 collection of the interlayer, which is difficult to visualize and obtain without leaving nuclei in

308 the gradient, leading to reduced yield. Nuclei pelleting with a sucrose gradient circumvents

309 these difficulties and allows nuclei resuspension in a buffer compatible with subsequent sorting

310 steps. We also found that a 10 min incubation in buffer before resuspension limited nuclei

311 rupture and clumping. Adding a filtration step just before sorting also decreased clumping

312 issues (Figure 2A).

B

IGEPAL	Nuclei (x10³/g)
0.1%	800
0.3%	300
0.5%	200

C

Dounce time (s)	Nuclei enrichment
15	77%
45	38%
75	35%
90	59%
105	100%

Nuclei aggregation

D

Dilution	Filtered nuclei
-	40%
1:3	45%
1:5	75%

313

314 Figure 2. *Nuclei isolation protocol*. (A) Snap frozen brain tissue is homogenized with a pestle

315 homogenizer. The sample is diluted before filtration and transferred to a sucrose gradient.

316 Nuclei are pelleted through centrifugation, filtered and immediately sorted using a Sony SH800

317 Cell Sorter. (B) Maximum number of nuclei obtained throughout homogenization with

318 different detergent concentrations. (C) Nuclei counts and aggregation increase with dounce

319 time, GFP$^+$ enrichment as percentage of the maximum number obtained. (D) Nuclei yield after

320   filtration increases with dilution, enrichment as percentage of the nuclei counted before

321   filtration.

322

323   For FANS, we first gated the majority of events detected in the forward and back scatter

324   channels, excluding larger events that could represent aggregated nuclei (Figure 3A). As an

325   alternative to the use of dyes like DAPI to detect and remove doublets and smaller clusters, we

326   plotted GFP signal intensity versus area using the population from the first gating (Figure 3B).

327   Singlets appear in the plot in a linear distribution, which were selected to exclude events below

328   the line (doublets) and close to the origin (GFP$^-$). These settings identify the population of

329   Sun1-GFP$^+$ nuclei singlets in the suspension without any additional treatment or manipulation

330   of the isolated nuclei. The gatings were optimized using GFP$^-$ samples, to further determine

331   the background levels of signal. Finally, to increase purity, a histogram of GFP signal was

332   plotted, and only events with highest fluorescence signal were collected (Figure 3C).

333   Samples collected before sorting and from GFP$^+$ or GFP$^-$ sorted nuclei were imaged to calculate

334   the extent of Sun1-GFP$^+$ nuclei enrichment. GFP signal was visible in Sun1-GFP sorted nuclei,

335   and no GFP signal was found in the gating for GFP$^-$ nuclei (Figure 3D). Our results indicate

336   that this method allows enrichment above 90% for astrocytes and microglia nuclei (Figure 3E).

337   We found that this high enrichment of GFP$^+$ nuclei depends heavily on the absence of nuclei

338   doublets or clusters. As an example, we determined enrichment for astrocyte nuclei with and

339   without the second gating for doublets and found that the purity of Sun1-GFP nuclei improved

340   by 10% when doublets and clusters were excluded (Figure 3F).

341

342

343

344
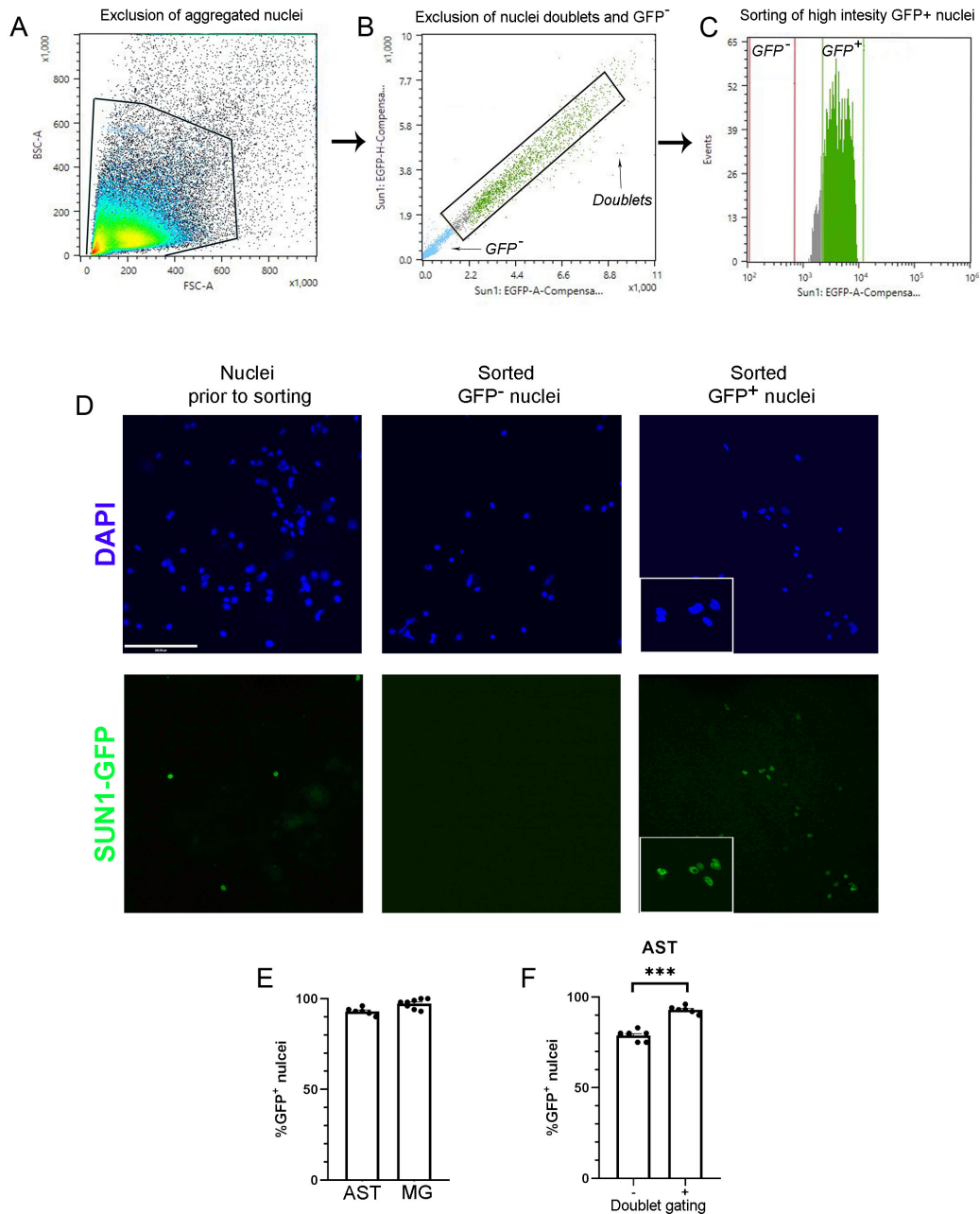
Figure 3. *High enrichment of GFP tagged nuclei obtained through FANS.* Representative images of the gating settings used to sort Sun1-GFP nuclei. (A) Gating set to discard clumps, events higher in the forward and back scattered channels; (B) population gated in A was then plotted according to EGFP signal intensity and area to identify nuclei singlets and remove doublets; (C) only nuclei singlets from the black box in B with higher EGFP signal intensity (shown in green) are collected, whereas events with lower EGFP signal (grey) are discarded.

352   (D) DAPI-stained nuclei obtained before sorting or from sorted GFP$^-$ and GFP$^+$ collection tubes

353   (E) Enrichment of Sun1-GFP$^+$ sorted astrocyte (AST) or microglia (MG) nuclei (mean +/-

354   SEM, n=6-8). (F) Enrichment of Sun1-GFP$^+$ sorted nuclei as % of GFP tagged nuclei for

355   astrocyte nuclei with or without gating to remove doublets, ***$p<0.0001$ unpaired t-test (n=6).

356

357   *3.2 RNA extraction yield and quality.*

358   To maintain high RNA quality and yield, we paused sorting a handful of times to vortex the

359   collection tube to ensure proper mixing of the nuclei in sheath solution with the lysis buffer.

360   Collection in the lysis buffer facilitates downstream processing, as lysis of the nuclei starts as

361   they are collected and does not require additional concentration steps before RNA extraction.

362   We also added 2-mercaptoethanol (2% final concentration) to the collection tube to account

363   for the volume of sheath solution containing the sorted nuclei. The RNA yield varied depending

364   on the type of cell: 70 – 240 ng of RNA for astrocytes, 170 – 370 ng for OPCs/oligodendrocytes

365   and 57 – 95 ng for microglia (Figure 4A). However, it is important to point out that these

366   numbers cannot be compared directly because the samples used for each cell type were

367   collected from different brain regions, at different time points. Moreover, each model uses

368   distinctive Cre driver lines with presumably different Cre expression. The regimen of

369   tamoxifen administration was also very different between animal models.

370   Interestingly, in the case of astrocytes and microglia, the amount of RNA obtained appears to

371   be determined by the cell type and not the number of nuclei. To better visualize the cell type-

372   specific differences in the RNA yield obtained, we calculated the amount of RNA per nuclei

373   and saw that microglia have significantly lower RNA content per nuclei and the results are less

374   variable compared to astrocytes and OPC/Oligodendrocytes (Figure 4B). These results indicate

375   that there might be cell type-specific differences in the RNA content in the nuclei of glial cells.

376   To validate the quality of RNA extraction, we selected astrocytes and OPC/Oligodendrocytes

377 for RIN analysis. Electrogram profiles and RIN from the Agilent bioanalyzer indicate that our

378 protocol produced high integrity RNA (Figure 4C), as all RNA samples are above the quality

379 threshold of a RIN above 7 for the glial cell types analyzed (Figure 4D). Therefore, despite

380 differences in RNA content, enough high-quality RNA for further transcriptomic analysis can

381 be obtained for each glial cell type with this method.

382

383
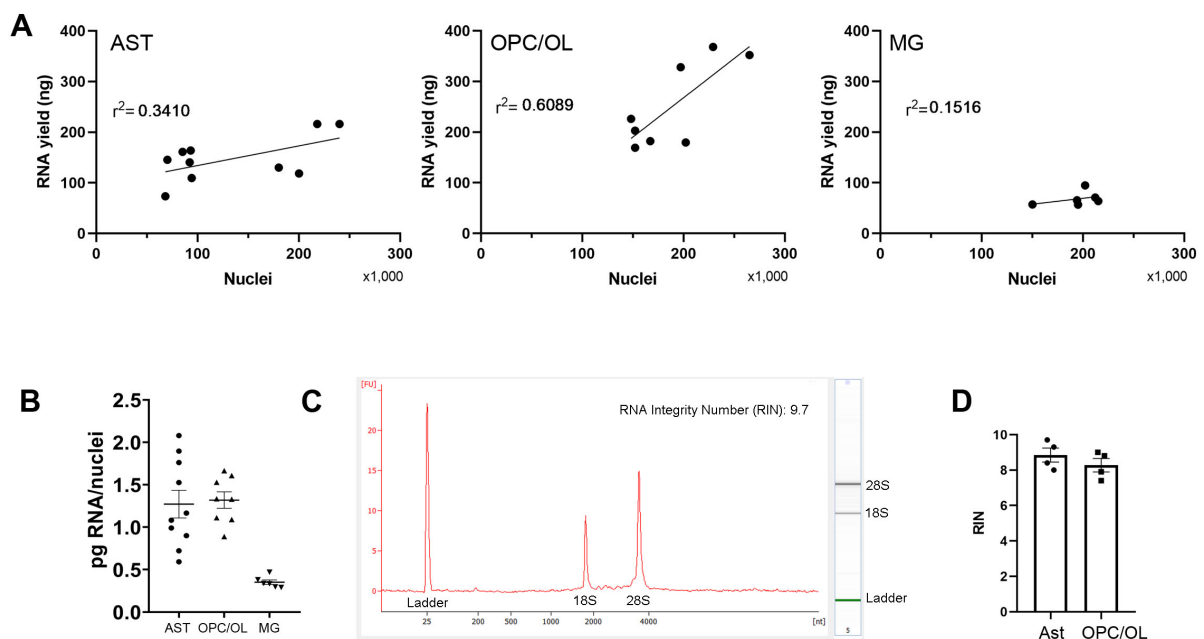
384

385 Figure 4. *High RNA yield and quality from Sun1-GFP nuclei obtained through FANS.* (A)

386 Correlation between RNA extracted from the respective nuclei collected for astrocytes (AST)

387 (p=0.0763), OPC/Oligodendrocytes (OPC/OLs) (p=0.0223) and microglia (MG) (p=0.4455).

388 (B) Calculated RNA content per nuclei obtained for every sorting session for each cell type

389 analyzed, ***p<0.0001 One-way ANOVA with Tukey's Multiple comparisons (AST n=10,

390 OPC/OL n=8, MG n=6). (C) Representative electrogram and gel view from Agilent

391 Bioanalyzer used for RIN analysis. (D) Quality of RNA extraction as shown in RIN values of

392 RNA samples extracted from astrocytes and OPC/OLs sorted nuclei (n=4).

393

394   *3.3 Cell type-specific gene expression and chromatin availability.*

395   We performed RNA-seq with three biological replicates using the RNA from sorted nuclei of

396   astrocytes, microglia, and OPC/Oligodendrocytes. To further validate our approach, we

397   compared the expression of well-known cell type-specific genes using the RNA-seq

398   transcriptome data. Hierarchical clustering of these genes shows that indeed, the cell type-

399   specific sets are enriched in their corresponding sample (Figure 5A). To further characterize

400   our enriched populations, we used sets of transcription factors differentially expressed in each

401   glial cell type, previously reported by Zhang et al., 2014 (Figure 5B), and observed distinct

402   enrichment for the corresponding glial cell type and appropriate clustering of the samples. We

403   also observe that astrocytes and OPC/Oligodendrocytes samples show higher similarity,

404   compared to microglia. The distinct clustering of each cell type based on gene expression

405   further validates that we obtained an enriched population of the desired glial cells, and that our

406   optimized method provides a useful tool to analyze the transcriptome of enriched nuclei

407   populations.

408   Astrocytes and microglia were selected for the validation of cell type-specific chromatin

409   accessibility on sorted nuclei. We therefore performed ATAC-seq with two biological

410   replicates using the sorted nuclei of astrocytes and microglia. To visualize the tracks of ATAC-

411   seq, we selected cell-type specific genes that showed differential gene expression in our RNA-

412   seq data. Consistent with cell type-specific gene expression, ATAC-seq also showed the

413   distinct cell type-specific chromatin accessibility peaks for microglia and astrocytes in selected

414   regions. For example, astrocytes specific genes *Aldh1l1*, *Aqp4* and *Gfap* showed more open

415   chromatin in astrocytes but not in microglia. Similarly, microglia specific genes *C1q*, *Csf1r*

416   and *Trem2* showed more open chromatin only in microglia (Figure 5C). Similar to the

417   transcriptomic results, chromatin accessibility assays reveal patterns characteristic of enriched

418   nuclei populations, confirming that our approach is suitable for omics analysis of the chromatin

419   as well as transcriptome.
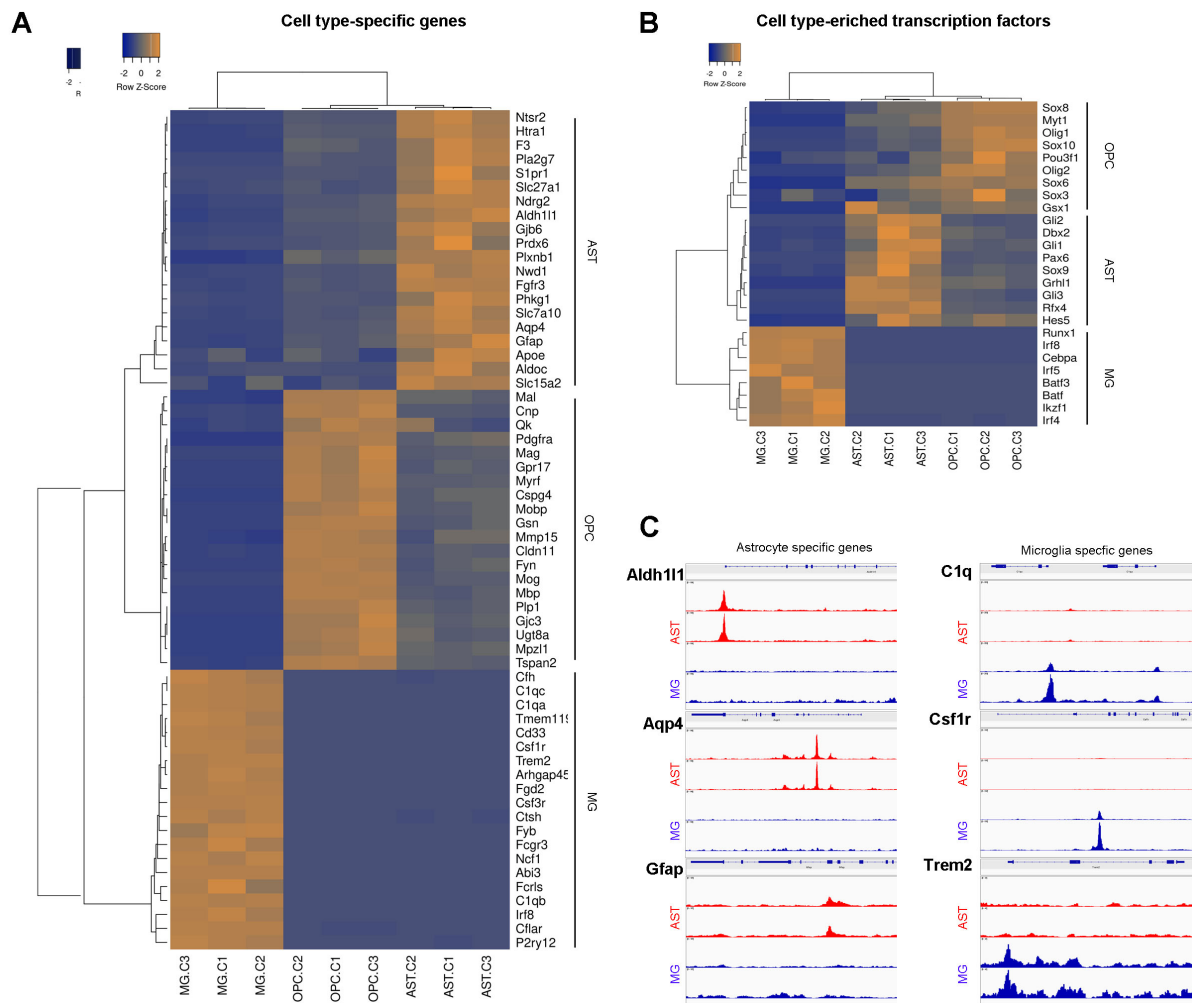
420

421   Figure 5. *Differential expression and chromatin availability of cell type-specific genes*

422   *determined by RNA-seq and ATAC-seq using sorted nuclei.* (A) Heatmap of RNA-seq

423   expression results with single linkage clustering and Spearman rank correlation shows higher

424   expression of the corresponding cell type-specific genes for astrocytes (AST),

425   OPC/Oligodendrocytes (OPC/OLs) and microglia (MG). (B) Enriched expression in the

426   corresponding glial cell of transcription factors reported in (Zhang et al., 2014) to be cell type-

427   enriched. (C) Chromatin availability from ATAC-seq analysis show distinct accessibility peak

428   pattern in cell type-specific genes with differential expression determined with RNA-seq.

429

430

4. CONCLUSION

432 We present an optimized method for nuclei isolation and sorting of fluorescently tagged nuclei,

433 applicable to a diverse population of cell types. Our method takes advantage of commercially

434 available mouse lines that allow fluorescent labelling of nuclei from a variety of cell types of

435 interest, avoiding the use of fixatives, antibodies or DNA dyes. The protocol used here for

436 nuclei isolation and sorting consists of optimized, rapid and fewer manipulation steps, avoids

437 cell dissociation stress while still yielding highly purified cell type-specific nuclei in sufficient

438 quantity and quality for omics applications. This optimized protocol will therefore be a useful

439 reference for the investigation of chromatin structure and gene expression in specific mouse

440 brain cell types of interest.

441

453

454

455

456

457

458 **Supplementary table 1: list of primer sequences**

Genotyping primer	Forward Sequence 5'→3'	Reverse Sequence 5'→3'
Sun1-GFP	AAG GGA GCT GCA GTG GAG TA	CGG GCC ATT TAC CGT AAG TTA T
Sox10-CreERT	CAC CTA GGG TCT GGC ATG T	CAG GTT TTG GTG CAC AGT CA
Glast-CreERT	ACA ATC TGG CCT GCT ACC AAA GC	CCA GTG AAA CAG CAT TGC TGT C
Cx3cr1-CreERT	AAG ACT CAC GTG GAC CTG CT	CGGTTATTCAACTTGCAC CA

459

460   **REFERENCES**
461

462   Allen, N.J., Eroglu, C., 2017. Cell Biology of Astrocyte-Synapse Interactions. Neuron 96, 697–708.
463   https://doi.org/10.1016/j.neuron.2017.09.056

464   Allen, N.J., Lyons, D.A., 2018. Glia as architects of central nervous system formation and function.
465   Science. https://doi.org/10.1126/science.aat0473

466   Babicki, S., Arndt, D., Marcu, A., Liang, Y., Grant, J.R., Maciejewski, A., Wishart, D.S., 2016.
467   Heatmapper: web-enabled heat mapping for all. Nucleic acids research 44, W147–W153.
468   https://doi.org/10.1093/nar/gkw419

469   Barres, B.A., 2014. Designing and troubleshooting immunopanning protocols for purifying neural
470   cells. Cold Spring Harbor Protocols 2014, 1342–1347. https://doi.org/10.1101/pdb.ip073999

471   Bayraktar, O.A., Fuentealba, L.C., Alvarez-Buylla, A., Rowitch, D.H., 2015. Astrocyte development and
472   heterogeneity. Cold Spring Harbor Perspectives in Biology 7.
473   https://doi.org/10.1101/cshperspect.a020362

474   Binek, A., Rojo, D., Godzien, J., Rupérez, F.J., Nunez, V., Jorge, I., Ricote, M., Vázquez, J., Barbas, C.,
475   2019. Flow Cytometry Has a Significant Impact on the Cellular Metabolome. Journal of
476   Proteome Research 18, 169–181. https://doi.org/10.1021/acs.jproteome.8b00472

477   Cahoy, J.D., Emery, B., Kaushal, A., Foo, L.C., Zamanian, J.L., Christopherson, K.S., Xing, Y., Lubischer,
478   J.L., Krieg, P.A., Krupenko, S.A., Thompson, W.J., Barres, B.A., 2008. A transcriptome database
479   for astrocytes, neurons, and oligodendrocytes: A new resource for understanding brain
480   development and function. Journal of Neuroscience 28, 264–278.
481   https://doi.org/10.1523/JNEUROSCI.4178-07.2008

482   Chongtham, M.C., Butto, T., Mungikar, K., Gerber, S., Winter, J., 2021. Intact vs. Fans for cell-type-
483   specific nuclei sorting: A comprehensive qualitative and quantitative comparison. International
484   Journal of Molecular Sciences 22. https://doi.org/10.3390/ijms22105335

485   Domingues, H.S., Portugal, C.C., Socodato, R., Relvas, J.B., 2016. Oligodendrocyte, astrocyte, and
486   microglia crosstalk in myelin development, damage, and repair. Frontiers in Cell and
487   Developmental Biology. https://doi.org/10.3389/fcell.2016.00071

488   Douvaras, P., Fossati, V., 2015. Generation and isolation of oligodendrocyte progenitor cells from
489   human pluripotent stem cells. Nature Protocols 10, 1143–1154.
490   https://doi.org/10.1038/nprot.2015.075

491   Durkee, C.A., Araque, A., 2019. Diversity and Specificity of Astrocyte–neuron Communication.
492   Neuroscience. https://doi.org/10.1016/j.neuroscience.2018.11.010

493   Eggen, B.J.L., Boddeke, E.W.G.M., Kooistra, S.M., 2019. Regulation of Microglia Identity from an
494   Epigenetic and Transcriptomic Point of View. Neuroscience.
495   https://doi.org/10.1016/j.neuroscience.2017.12.010

496   Foo, L.C., Allen, N.J., Bushong, E.A., Ventura, P.B., Chung, W.S., Zhou, L., Cahoy, J.D., Daneman, R.,
497   Zong, H., Ellisman, M.H., Barres, B.A., 2011. Development of a method for the purification and
498   culture of rodent astrocytes. Neuron 71, 799–811.
499   https://doi.org/10.1016/j.neuron.2011.07.022

Guez-Barber, D., Fanous, S., Harvey, B.K., Zhang, Y., Lehrmann, E., Becker, K.G., Picciotto, M.R., Hope, B.T., 2012. FACS purification of immunolabeled cell types from adult rat brain. Journal of Neuroscience Methods 203, 10–18. https://doi.org/10.1016/j.jneumeth.2011.08.045

Hammond, T.R., Dufort, C., Dissing-Olesen, L., Giera, S., Young, A., Wysoker, A., Walker, A.J., Gergits, F., Segel, M., Nemesh, J., Marsh, S.E., Saunders, A., Macosko, E., Ginhoux, F., Chen, J., Franklin, R.J.M., Piao, X., McCarroll, S.A., Stevens, B., 2019. Single-Cell RNA Sequencing of Microglia throughout the Mouse Lifespan and in the Injured Brain Reveals Complex Cell-State Changes. Immunity 50, 253-271.e6. https://doi.org/10.1016/j.immuni.2018.11.004

Holt, L.M., Olsen, M.L., 2016. Novel applications of magnetic cell sorting to analyze cell-type specific gene and protein expression in the central nervous system. PLoS ONE 11. https://doi.org/10.1371/journal.pone.0150290

Jiang, Y., Matevossian, A., Huang, H.S., Straubhaar, J., Akbarian, S., 2008. Isolation of neuronal chromatin from brain tissue. BMC Neuroscience 9. https://doi.org/10.1186/1471-2202-9-42

John Lin, C.C., Yu, K., Hatcher, A., Huang, T.W., Lee, H.K., Carlson, J., Weston, M.C., Chen, F., Zhang, Y., Zhu, W., Mohila, C.A., Ahmed, N., Patel, A.J., Arenkiel, B.R., Noebels, J.L., Creighton, C.J., Deneen, B., 2017. Identification of diverse astrocyte populations and their malignant analogs. Nature Neuroscience 20, 396–405. https://doi.org/10.1038/nn.4493

Lattke, M., Goldstone, R., Ellis, J.K., Boeing, S., Jurado-Arjona, J., Marichal, N., MacRae, J.I., Berninger, B., Guillemot, F., 2021. Extensive transcriptional and chromatin changes underlie astrocyte maturation in vivo and in culture. Nature Communications 12. https://doi.org/10.1038/s41467-021-24624-5

Maitra, M., Nagy, C., Chawla, A., Wang, Y.C., Nascimento, C., Suderman, M., Théroux, J.F., Mechawar, N., Ragoussis, J., Turecki, G., 2021. Extraction of nuclei from archived postmortem tissues for single-nucleus sequencing applications. Nature Protocols. https://doi.org/10.1038/s41596-021-00514-4

Marek, R., Caruso, M., Rostami, A., Grinspan, J.B., Sarma, J. das, 2008. Magnetic cell sorting: A fast and effective method of concurrent isolation of high purity viable astrocytes and microglia from neonatal mouse brain tissue. Journal of Neuroscience Methods 175, 108–118. https://doi.org/10.1016/j.jneumeth.2008.08.016

Marques, S., van Bruggen, D., Vanichkina, D.P., Floriddia, E.M., Munguba, H., Väremo, L., Giacomello, S., Falcão, A.M., Meijer, M., Björklund, Å.K., Hjerling-Leffler, J., Taft, R.J., Castelo-Branco, G., 2018. Transcriptional Convergence of Oligodendrocyte Lineage Progenitors during Development. Developmental Cell 46, 504-517.e7. https://doi.org/10.1016/j.devcel.2018.07.005

Marques, S., Zeisel, A., Codeluppi, S., van Bruggen, D., Falcão, A.M., Xiao, L., Li, H., Häring, M., Hochgerner, H., Romanov, R.A., Gyllborg, D., Muñoz-Manchado, A.B., la Manno, G., Lönnerberg, P., Floriddia, E.M., Rezayee, F., Ernfors, P., Arenas, E., Hjerling-Leffler, J., Harkany, T., Richardson, W.D., Linnarsson, S., Castelo-Branco, G., 2016. Oligodendrocyte heterogeneity in the mouse juvenile and adult central nervous system. Science 352, 1326–1329. https://doi.org/10.1126/science.aaf6463

Matejuk, A., Ransohoff, R.M., 2020. Crosstalk Between Astrocytes and Microglia: An Overview. Frontiers in Immunology. https://doi.org/10.3389/fimmu.2020.01416

542 Matias, I., Morgado, J., Gomes, F.C.A., 2019. Astrocyte Heterogeneity: Impact to Brain Aging and
543   Disease. Frontiers in Aging Neuroscience. https://doi.org/10.3389/fnagi.2019.00059

544 Maze, I., Shen, L., Zhang, B., Garcia, B.A., Shao, N., Mitchell, A., Sun, H.S., Akbarian, S., Allis, C.D.,
545   Nestler, E.J., 2014. Analytical tools and current challenges in the modern era of
546   neuroepigenomics. Nature Neuroscience. https://doi.org/10.1038/nn.3816

547 McKenzie, I.A., Ohayon, D., Li, H., de Faria, J.P., Emery, B., Tohyama, K., Richardson, W.D., 2014.
548   Motor skill learning requires active central myelination. Science 346, 318–322.
549   https://doi.org/10.1126/science.1254960

550 Mendizabal, I., Berto, S., Usui, N., Toriumi, K., Chatterjee, P., Douglas, C., Huh, I., Jeong, H., Layman,
551   T., Tamminga, C.A., Preuss, T.M., Konopka, G., Yi, S. v., 2019. Cell type-specific epigenetic links
552   to schizophrenia risk in the brain. Genome Biology 20. https://doi.org/10.1186/s13059-019-
553   1747-7

554 Mo, A., Mukamel, E.A., Davis, F.P., Luo, C., Henry, G.L., Picard, S., Urich, M.A., Nery, J.R., Sejnowski,
555   T.J., Lister, R., Eddy, S.R., Ecker, J.R., Nathans, J., 2015. Epigenomic Signatures of Neuronal
556   Diversity in the Mammalian Brain. Neuron 86, 1369–1384.
557   https://doi.org/10.1016/j.neuron.2015.05.018

558 Nott, A., Holtman, I.R., Coufal, N.G., Schlachetzki, J.C.M., Yu, M., Hu, R., Han, C.Z., Pena, M., Xiao, J.,
559   Wu, Y., Keulen, Z., Pasillas, M.P., O'Connor, C., Nickl, C.K., Schafer, S.T., Shen, Z., Rissman, R.A.,
560   Brewer, J.B., Gosselin, D., Gonda, D.D., Levy, M.L., Rosenfeld, M.G., McVicker, G., Gage, F.H.,
561   Ren, B., Glass, C.K., 2019. Brain cell type–specific enhancer–promoter interactome maps and
562   disease-risk association. Science 366, 1134–1139. https://doi.org/10.1126/science.aay0793

563 Nutma, E., van Gent, D., Amor, S., Peferoen, L.A.N., 2020. Astrocyte and Oligodendrocyte Cross-Talk
564   in the Central Nervous System. Cells. https://doi.org/10.3390/cells9030600

565 Parkhurst, C.N., Yang, G., Ninan, I., Savas, J.N., Yates, J.R., Lafaille, J.J., Hempstead, B.L., Littman, D.R.,
566   Gan, W.B., 2013. Microglia promote learning-dependent synapse formation through brain-
567   derived neurotrophic factor. Cell 155, 1596–1609. https://doi.org/10.1016/j.cell.2013.11.030

568 Reemst, K., Noctor, S.C., Lucassen, P.J., Hol, E.M., 2016. The indispensable roles of microglia and
569   astrocytes during brain development. Frontiers in Human Neuroscience 10.
570   https://doi.org/10.3389/fnhum.2016.00566

571 Sakry, D., Karram, K., Trotter, J., 2011. Synapses between NG2 glia and neurons. Journal of Anatomy.
572   https://doi.org/10.1111/j.1469-7580.2011.01359.x

573 Sakry, D., Neitz, A., Singh, J., Frischknecht, R., Marongiu, D., Binamé, F., Perera, S.S., Endres, K., Lutz,
574   B., Radyushkin, K., Trotter, J., Mittmann, T., 2014. Oligodendrocyte Precursor Cells Modulate
575   the Neuronal Network by Activity-Dependent Ectodomain Cleavage of Glial NG2. PLoS Biology
576   12. https://doi.org/10.1371/journal.pbio.1001993

577 Slezak, M., Göritz, C., Niemiec, A., Frisén, J., Chambon, P., Metzger, D., Pfrieger, F.W., 2007.
578   Transgenic mice for conditional gene manipulation in astroglial cells. GLIA 55, 1565–1576.
579   https://doi.org/10.1002/glia.20570

580 Tiane, A., Schepers, M., Rombaut, B., Hupperts, R., Prickaerts, J., Hellings, N., van den Hove, D.,
581   Vanmierlo, T., 2019. From OPC to Oligodendrocyte: An Epigenetic Journey. Cells.
582   https://doi.org/10.3390/cells8101236

583 Vainchtein, I.D., Molofsky, A. v., 2020. Astrocytes and Microglia: In Sickness and in Health. Trends in
584   Neurosciences. https://doi.org/10.1016/j.tins.2020.01.003

585 Xin, W., Chan, J.R., 2020. Myelin plasticity: sculpting circuits in learning and memory. Nature Reviews
586   Neuroscience. https://doi.org/10.1038/s41583-020-00379-8

587 Zhang, Y., Chen, K., Sloan, S.A., Bennett, M.L., Scholze, A.R., O'Keeffe, S., Phatnani, H.P., Guarnieri, P.,
588   Caneda, C., Ruderisch, N., Deng, S., Liddelow, S.A., Zhang, C., Daneman, R., Maniatis, T., Barres,
589   B.A., Wu, J.Q., 2014. An RNA-sequencing transcriptome and splicing database of glia, neurons,
590   and vascular cells of the cerebral cortex. Journal of Neuroscience 34, 11929–11947.
591   https://doi.org/10.1523/JNEUROSCI.1860-14.2014

592